*Pol. J. Environ. Stud. Vol. 35, No. 4 (2026), 4575-4586*
DOI: *10.15244/pjoes/207656* ONLINE PUBLICATION DATE: 2025-08-08

*Original Research*

# Camel Bone-Derived Hydroxyapatite as Green Adsorbent for Methylene Blue Dye

**Raiedhah A. Alsaiari***

Department of Chemistry, College of science and art in Sharurah, Najran University, Saudi Arabia

*Received: 15 December 2024*
*Accepted: 27 June 2025*

## Abstract

This study explores the feasibility of using camel bone-derived hydroxyapatite as a cost-effective adsorbent for removing methylene blue dye from aqueous solutions. The adsorbent was synthesized through calcination and characterized using BET, XRD, and TEM, confirming its crystalline structure and porous surface. Adsorption performance was evaluated under varying conditions, including contact time, adsorbent dosage, and dye concentration. The maximum adsorption capacity was found to be 23 mg/g, following the Langmuir isotherm model ($R^2$ = 0.9894), confirming monolayer adsorption. Kinetic analysis indicated that the adsorption followed the pseudo-second-order model, with a rate constant of 0.0021 g/mg·min and an equilibrium adsorption capacity of 23.15 mg/g. Thermodynamic parameters revealed an endothermic process ($\Delta H$ = 16614J/mol) driven by entropy gain ($\Delta S°$ = 64 J/mol·K) and spontaneous adsorption as reflected by negative $\Delta G°$ values (-9826 J/mol to -12066 J/mol in the temperature range of 303-363 K). The material maintained high efficiency across multiple reuse cycles, with 98% removal efficiency at an optimized temperature of 50ºC, highlighting its potential for sustainable wastewater treatment applications.

**Keywords**: hydroxyapatite, camel bone, methylene blue dye, adsorption, isotherm model, kinetics study

## Introduction

The global dye industry produces substantial amounts of colored effluents, resulting in considerable ecological impacts. Various industrial sectors, such as textile manufacturing, paper and pulp processing, dye synthesis, electroplating, distillation, and the production of rubber, plastics, leather, food, and pharmaceuticals, are responsible for the discharge of colored wastewater [1-4]. The release of these effluents into the environment raises issues owing to their intrinsic toxicity and the visual pollution they create in aquatic environments [5-7]. Azo dyes are notably resistant, non-biodegradable, and durable among the several types of dyes [8].

Numerous techniques have been established for extracting dyes from wastewater, including chemical oxidation, ion exchange, adsorption, ultrafiltration, photocatalysis, electrodialysis, coagulation-flocculation, and catalytic degradation [9-12]. Among them, adsorption is acknowledged as a synergistic physicochemical technique that is both efficient and economical for removing dyes from aqueous solutions [13]. Dye removal processes rely heavily on a variety of natural adsorbents, including activated carbon, agricultural by-products such as corn husk, coniferous biomass, jute fiber, wheat shell, rice husk, bamboo dust,

*e-mail: raalsayari@nu.edu.sa

© 2026 This article is licensed under a Creative Commons Attribution-NonCommercial 4.0 International (CC BY-NC 4.0)

sugarcane by-products, zeolites, and carbonaceous materials derived from bituminous clays [14].

Within the framework of wastewater treatment, materials derived from animal bone have shown notable adsorptive capacity for both dyes and heavy metals [15]. Well-known for its environmental properties is hydroxyapatite (HAp), a naturally occurring mineral made of calcium apatite with the chemical formula $Ca_{10}(PO_4)_6(OH)_2$. It has several possible uses in removing pollutants and is non-toxic and biocompatible [16, 17]. This bioactive material can now be produced from biological waste or via economical chemical synthesis techniques due to advancements in materials science and nanotechnology. Because of its structural adaptability, thermal and chemical stability, and very low water solubility (Kps ≈ 10-59 at 25ºC), HAp is a powerful sorbent for a variety of inorganic pollutants. Mechanisms including surface complexation, ion exchange, and dissolution-precipitation are responsible for this effectiveness [18]. Barua et al. extracted hydroxyapatite from bovine bone debris and examined the bioactivity and biodegradability of the resultant bone scaffold [19].

Camel bones (CB), which are abundantly available in arid regions such as the Empty Quarter desert, represent a major source of biological waste. Their improper disposal not only contributes to environmental degradation but also poses public health risks due to bacterial proliferation from residual organic matter. Converting this waste into hydroxyapatite (HAp) provides a sustainable and eco-conscious approach to pollution mitigation. Unlike bovine, fish, or poultry bones, which have been more extensively studied, camel bone remains underexplored as a precursor for HAp synthesis. Its unique availability in desert climates makes it particularly attractive for localized wastewater treatment efforts. This study aims to fill that gap by synthesizing HAp from waste camel bone and evaluating its efficacy for methylene blue (MB) dye removal. The proposed approach contributes to both waste valorization and environmental remediation, offering a dual benefit of cost-effective dye removal and sustainable waste management.

## Materials and Methods

The methylene blue dye ($C_{16}H_{18}ClN_3S$) used in this study was purchased from Sigma-Aldrich (≥98% purity, USA) and used without further purification. Analytical-grade sodium hydroxide (NaOH, 99% purity, Merck, Germany) and hydrochloric acid (HCl, 37% purity, Sigma-Aldrich, USA) were used for pH adjustment. Deionized water was used throughout all experiments.

### Synthesis and Analysis of the Adsorbent

Waste camel bones were obtained from a local restaurant in Sharurah, Saudi Arabia, and used as the raw material for hydroxyapatite synthesis. The bones were first cleaned thoroughly using hot deionized water and then sun-dried for 24 hours before being oven-dried at 120ºC for 6 hours. The dried bones were subsequently calcined in a muffle furnace (Nabertherm GmbH, Germany) at temperatures ranging from 600 to 1100ºC for 3 hours at a heating rate of 10ºC/min.

Brunauer–Emmett–Teller (BET) Surface Area Analysis: The specific surface area, pore volume, and pore size distribution of the adsorbent were determined using a Micromeritics ASAP 2020 analyzer (Micromeritics Instrument Corp., USA).

X-Ray Diffraction (XRD) Analysis: The crystalline structure of the adsorbent was examined using an X-ray diffractometer (PANalytical X'Pert Pro, Netherlands) with Cu Kα radiation (λ = 1.5406 Å) at a scanning rate of 2º/min.

Transmission Electron Microscopy (TEM): The morphological characteristics and particle size were observed using a JEOL JEM-2100 (JEOL Ltd., Japan) operating at an accelerating voltage of 200 kV.

Fourier Transform Infrared Spectroscopy (FTIR): Functional groups were analyzed using an FTIR spectrometer (Thermo Scientific Nicolet iS50, USA) in the range of 4000-400 $cm^{-1}$.

Ultraviolet-Visible (UV-Vis) Spectroscopy: The concentration of methylene blue dye was determined using a UV-Vis spectrophotometer (Shimadzu UV-1800, Japan) at a wavelength of 670 nm.

pH Measurement: The solution pH was adjusted and monitored using a pH meter (Mettler Toledo SevenCompact S220, Switzerland).

### Batch Adsorption Process

The tests were conducted using a magnetic orbital shaker, with the contents placed in a 100 mL conical flask. The experiment was conducted in triplicate, yielding an average result. The effects of methylene blue concentration were examined within the range of 25 to 200 mg $L^{-1}$, camel bone dosage from 0.25 to 1 g, duration from 20 to 100 minutes, and solution pH from 2.0 to 7.0. In 25 mL of MB solution, 40 mg of the camel bone was added momentarily. The solution's pH was adjusted to the desired value by adding 0.1 M NaOH or HCl after equilibration on the orbital shaker. At various points in time, a certain quantity of MB was extracted and examined using an ultraviolet-visible spectrophotometer set to 670 nm. Using the following relationship, the equilibrium quantity of MB adsorbed by the synthesized hydroxyapatite was calculated:

$$q_{e=} \frac{c_0 - c_e}{W} XV \quad (1)$$

Considering that $C_0$ and $C_e$ (mg/L) represent the initial and equilibrium concentrations of methylene blue (MB), respectively, V denotes the solution volume in liters, and W refers to the mass of hydroxyapatite

used, measured in milligrams. The removal percentage (R%) of methylene blue (MB) was calculated using the following Equation:

$$\text{Removal } \% = \frac{c_o - c_e}{C_0} x100 \quad (2)$$

The adsorption experiments were methodically altered by modifying the initial concentration of methylene blue dye (from 5 ppm to 50 ppm), the quantity of adsorbent employed (from 0.2 g to 1 g), the solution pH (from 2 to 9), the reaction duration (30 minutes to 120 minutes), and the temperature (between 33ºC and 80ºC) to determine the optimal conditions for dye elimination.

## Results and Discussion

### Adsorbent Characterizations

#### *BET*

Table 1 displays the average pore diameter, specific surface area, and specific pore volume of the catalyst samples calcined at varying temperatures. Using XRD (Fig. 1), it is evident that increasing the calcination temperature resulted in a loss of specific surface area among these materials. This may be related to the fact that the adsorbent materials calcined at higher temperatures have better crystalline order. In addition, compared to previous methods, the camel bone calcined at 1100ºC exhibited a smaller pore diameter. Microporous materials exhibit the shown pore sizes.

#### *XRD Analysis*

XRD analysis confirmed the presence of characteristic basal peaks of hydroxyapatite in all materials calcined at different temperatures, indicating improved crystalline ordering [20].

Table 1. BET analysis of the camel bone catalyst subjected to various calcination temperatures.

| Hydroxyapatite (camel bone) calcined at a range of calcination temperatures | Surface area ($m^2/g$) | Size of Pore (nm) | Volume of Pore ($cm^3/g$) |
|---|---|---|---|
| 700 | 19.6 | 6.8 | 0.067 |
| 900 | 15.7 | 2.99 | 0.023 |
| 1100 | 15.5 | 2.29 | 0.019 |

#### *TEM*

TEM analysis was used to examine the particle size of the hydroxyapatite catalyst, revealing irregularly shaped grains with an average size ranging from approximately 1.2 nm to 10 µm. The adsorbent particles did not exhibit a clearly defined hexagonal shape, consistent with the XRD results, likely due to agglomeration in certain regions (Fig. 2).

### Effect of Initial Methylene Blue Dye Concentration

The adsorption capacity of adsorbent nanocomposites is significantly influenced by the initial dye concentration. The adsorption behavior of the methylene blue dye was investigated in a concentration range of 30 mg/L to 100 mg/L at 50°C, with the adsorbent concentration maintained at 0.75 g for 60 minutes, as illustrated in Fig. 3. The nanocomposite's adsorption capability correlated positively with larger initial methylene blue dye concentrations due to

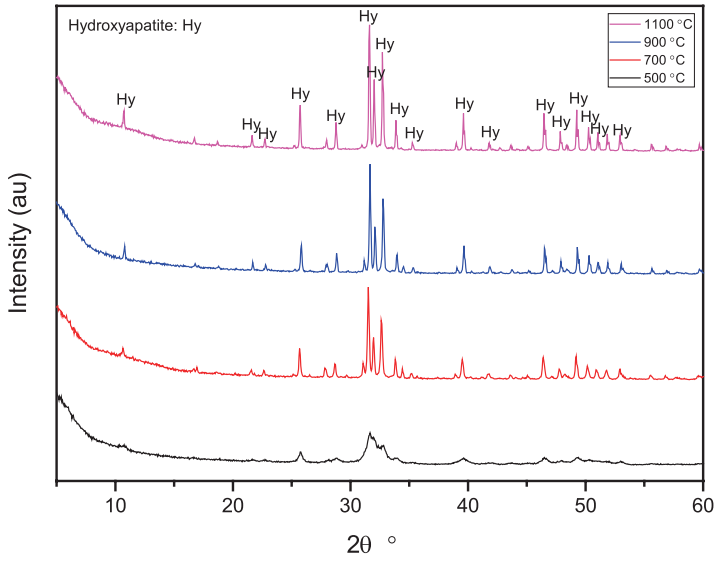


Fig. 1. XRD analysis of hydroxyapatite catalysts synthesized from waste camel bone and calcined at varying temperatures.

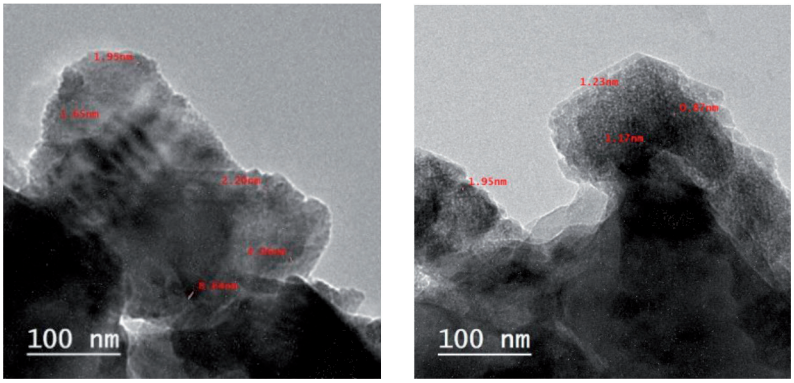


Fig. 2. TEM image of calcined hydroxyapatite derived from waste camel bone.

the increased mass transfer driving force. Higher dye concentrations (100 mg/L) mark a saturation point in adsorption capacity, therefore showing the saturation of the accessible adsorption sites on the nanocomposite. A similar adsorption ability of activated palm ash against acid dye was found in a previous study. [21, 22].

## Effect of Adsorbent Dosage

The impact of hydroxyapatite nanocomposite dose on methylene blue dye removal was investigated by varying the dosage from 0.25 g to 1 g at 50°C for 60 minutes while maintaining a constant dye concentration (50 mg/L). The dose of the hydroxyapatite nanocomposite greatly influences the effectiveness of dye removal. Fig. 4 illustrates how adsorption experiments reveal that the proportion of methylene blue dye removal increases with rising adsorbent doses, which can be attributed to the availability of greater adsorption sites and a higher adsorbent surface area. This effect is most apparent at lower concentrations; however, it gradually diminishes as the dosage increases from 0.25 to 1 g. At higher dosages (1 g), the adsorbent particles may aggregate, resulting in a decrease in effective surface area and a decrease in adsorption capacity [23, 24]. This behavior has been observed in a variety of sorbate and sorbent combinations. Initially, the adsorbent has access to all of the dye's interaction sites. The number of unoccupied interaction sites in the dye decreases and ultimately reaches saturation as the concentration of hydroxyapatite in the solution increases. The reduction of $q_e$ from 192 mg/g to 49 mg/g with an increase in adsorbent dosage from 0.25 g to 1 g was attributable to the competition between adsorption and the separation induced by the concentration gradient. One explanation is that increasing the adsorbent dosage will prevent the adsorption process from saturating adsorption sites at a given methylene blue dye concentration and volume [15, 17]. Simultaneously, the adsorbent's particle aggregation would result in a decrease in its capacity as it increases the diffusional path length and decreases the total surface area.

## Effect of Reaction Time

Fig. 5 illustrates the correlation between methylene blue adsorption capacity and time, as well as between methylene blue adsorption efficiency and time. As seen

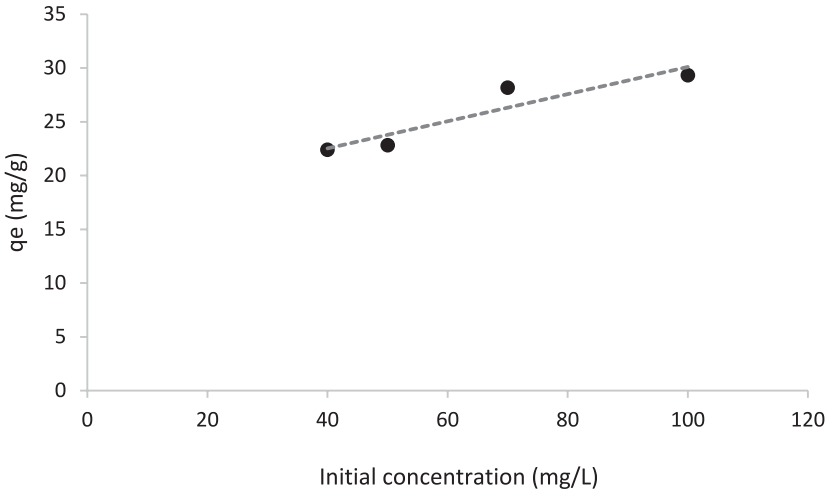


Fig. 3. Adsorption capacity of camel bone-derived hydroxyapatite at varying initial methylene blue concentrations.

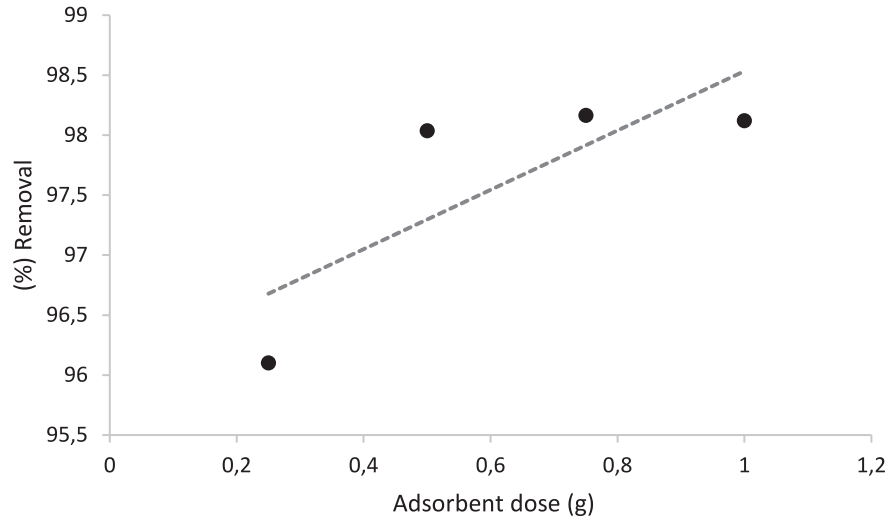


Fig. 4. Effect of adsorbent dose on methylene blue removal.

in Fig. 5, MB's adsorption capacity and efficiency increased with time. The camel bone MB adsorption process is divided into two phases: the first reaction step, extending from the 1st to the 30th minute, followed by the subsequent stage. Surface adsorption was the primary mechanism of the first-stage reaction, which enhanced adsorption efficiency and capacity while also speeding up the adsorption process [21, 25]. The adsorption process occurred at a somewhat moderate pace, with gradual adsorption dominating the second stage of the reaction. It took 90 to 120 minutes to progressively attain equilibrium. Because of the mesoporous material's strong mass transfer driving force in the early stages of adsorption and its availability of active sites, MB may be easily absorbed by the camel bone. Over time, MB builds up on the surface of the camel bone, causing nonlinear adsorption that reduces the number of active sites and impairs MB mobility.

## Effect of Reaction Temperature

Temperature is an important component that affects the adsorption process, as it controls the diffusion rate of adsorbate molecules and the adsorbent's equilibrium capacity [26]. Fig. 6 shows the adsorption of methylene blue dye with the hydroxyapatite nanocomposite at temperatures ranging from 30°C to 90°C. The adsorbent dose, initial dye concentration, and solution pH were maintained at 0.75 g, 50 mg/L, and 10, respectively. The findings indicate that optimum adsorption (98%) is achieved at 50°C, after which a decrease in adsorption effectiveness is seen. The first rise in adsorption with temperature may be explained by the dye molecules' increased kinetic energy and a possible swelling effect within the internal structure of the nanocomposite, which allows the dye molecules to penetrate deeper [27]. Reduced adsorption might nevertheless arise from weakening adsorptive interactions between the active

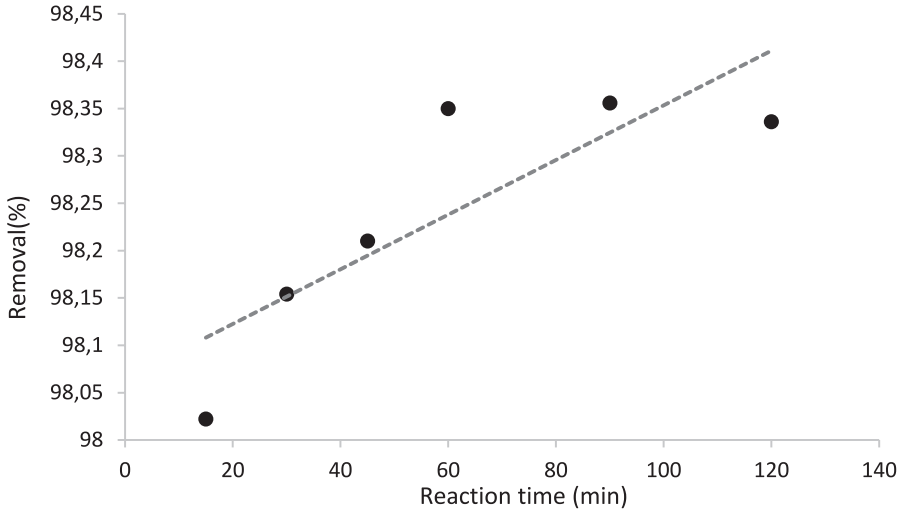


Fig. 5. Effect of reaction time on methylene blue removal.

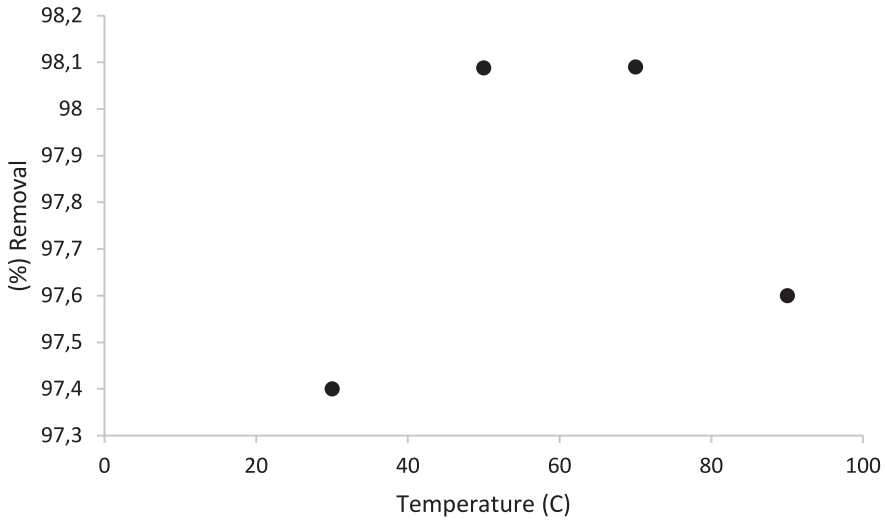


Fig. 6. Effect of reaction temperature on methylene blue removal.

sites on the nanocomposite and the dye at temperatures above 50ºC.

To evaluate the practical relevance of camel bone-derived HAp, its adsorption efficiency was compared with other adsorbents reported in the literature. As shown in Table 2, the maximum monolayer adsorption capacity of camel bone-HAp for methylene blue (MB) was 23 mg/g, which is comparable to bovine bone-derived HAp in other studies.

The production of hydroxyapatite from camel bone waste offers significant environmental and economic advantages for wastewater treatment. The sustainability benefit lies in diverting biowaste from landfills, reducing methane emissions, and transforming a waste stream into a functional, reusable material for water treatment. This positions camel bone-derived HAp as not only a technically effective adsorbent but also a viable solution for localized, low-cost wastewater treatment infrastructure.

## Adsorption Isotherms

The adsorption process of MB solution onto hydroxyapatite was modeled by fitting the adsorption data to the Langmuir and the Freundlich isotherm models [28]. The Langmuir and Freundlich isothermal Equations are as follows:

$$\frac{C_e}{q_e} = \frac{1}{q_{max}.b} + \frac{1}{q_{max}} .Ce \quad (3)$$

$$\ln q_e = \ln K_f + \frac{1}{n} \ln C_e \quad (4)$$

Where $q_e$ denotes the adsorption capacity at equilibrium (mg/g) and Ce represents the equilibrium concentration (mg/L); where b is the Langmuir constant related to adsorption capacity (mg/g), while $q_{max}$ represents the maximum adsorption capacity (mg/g); where n denotes the adsorption intensity, and $K_f$ is the Freundlich constant (L/mg).

The $C_e/q_e$ vs. Ce plot, as shown in Fig. 7a), was used to determine the Langmuir isotherm parameters, which produced correlation coefficients ($R^2$) of 0.9894. These coefficients confirm that the Langmuir model is appropriate for the adsorption system under investigation. With matching Langmuir constants of 0.07 L/mg, the calculated monolayer adsorption capacities were 23 mg/g (see Table 2).

A dimensionless equilibrium factor ($R_L$) can be used to express the fundamental characteristics of the

Table 2. Comparison of the adsorption capacity of camel bone with other adsorbents.

| Adsorbent Type | Source Material | q (mg/g) | Reference |
|---|---|---|---|
| Camel bone HAp | Camel bone waste | 23 | This study |
| Bovine bone HAp | Bovine bone | 18-22 | [28] |
| Fishbone HAp | Fish bone waste | 19.4 | [29] |
| Eggshell-derived HAp | Eggshells | 17-20 | [4] |
| Biochar (sugarcane bagasse) | Agro waste | 12-25 | [30] |
| Zeolites | Natural minerals | 10-25 | [31] |

Langmuir isotherm. The definition of this parameter is as follows:

$$R_L = \frac{1}{bCi} \quad (5)$$

where Ci is the initial concentration of methylene blue dye, and the $R_L$ value indicates whether the adsorption is unfavorable: $R_L$>1; linear: $R_L$ = 1; favorable: 0< $R_L$<1; or irreversible: $R_L$ = 0. The Langmuir isotherm was confirmed as the best model for describing the adsorption of methylene blue, as RL was found to be less than 1.

The adsorbate also influences them when n is between 1 and 10 (1/n is less than 1). Adsorption is believed to be enhanced by n values ranging from 1 to 10, with n>1 being the most common [29], elucidating the distribution of active sites on the surface or any other factor that leads to a reduction in the adsorbent-adsorbate interaction as surface density rises. The values of $K_f$ and n were derived from the slope and intercept of the graph plotting ln $C_e/q_e$ versus ln Ce, as seen in Fig. 7b). With an $R^2$ value of 0.8852, the Freundlich model produced a good match for the methylene blue dye adsorption. It was found that the obtained Freundlich constants were $K_f$ = 2.3 and n = 4, as shown in Table 3.

The Langmuir model is clearly superior to the Freundlich model based on the correlation coefficients; therefore, the adsorption process is initially a single-layer adsorption process. The Freundlich isotherm model describes the heterogeneity factor and adsorption intensity; the anticipated heterogeneity increases with decreasing 1/n.

## Adsorption Kinetics

When assessing the mechanism and effectiveness of the sorption process, understanding the physical or chemical interactions between the adsorbent and adsorbate is crucial. Adsorption kinetics provide

Table 3. Parameters of Langmuir and Freundlich isotherms of MB.

| Isotherm model | Evaluated parameters of isotherms | | |
|---|---|---|---|
| Langmuir | $q_{max}$ (mg/g) | b (L/mg) | $R^2$ |
| | 23 | 0.07 | 0.9894 |
| Freundlich | n | $K_f$ | $R^2$ |
| | 4 | 2.3 | 0.8852 |

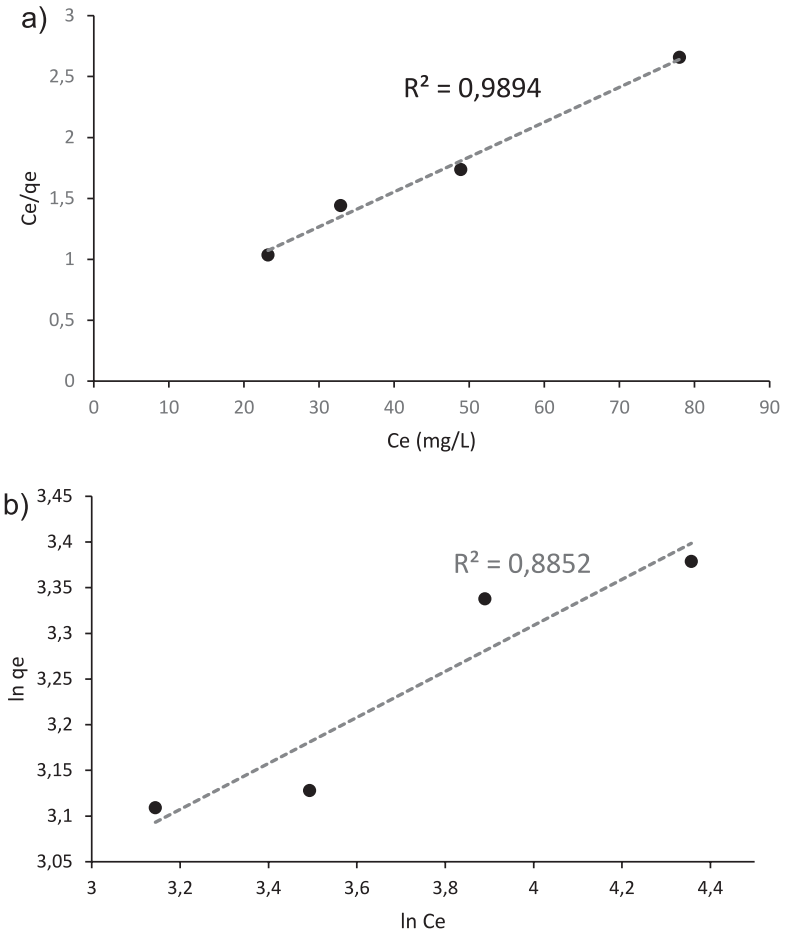


Fig. 7. Linear fits of the adsorption of methylene blue on camel bone predicted by various isotherm models. a) Langmuir b) Freundlich.

essential details about these interactions. The kinetic process was described using pseudo-first-order and pseudo-second-order models independently in order to investigate the mechanism of methylene blue dye adsorption on hydroxyapatite. The linear form of the pseudo-first-order model is expressed as follows, as it was initially proposed:

$$\ln(q_e - q_t) = \ln q_e - k_1 t \quad (6)$$

Where $k_1$ is the pseudo-first-order rate constant ($min^{-1}$), $q_t$ represents the adsorption capacity at time t (mg/g), and $q_e$ denotes the adsorption capacity at equilibrium (mg/g).

The pseudo-second-order kinetics model can be expressed in its linearized form as follows:

$$\frac{t}{q_t} = \frac{1}{k_2 q_e^2} + \frac{t}{q_e} \quad (7)$$

Where $q_e$ and $q_t$ (mg/g) indicate the equilibrium and time-dependent adsorption capacities, respectively, while $k_2$ (g/mg min) represents the rate constant of the pseudo-second-order kinetics.

Based on the calculated experimental adsorption capacity ($q_e$) of 23.0 mg/g, a comparative analysis was performed between the pseudo-first-order and pseudo-second-order kinetic models to determine the best fit for the adsorption process of methylene blue onto camel bone-derived adsorbent. The theoretical $q_e$ value predicted by the pseudo-first-order model was approximately 16 mg/g, which significantly deviates from the experimentally obtained value, indicating a poor fit for the adsorption kinetics (Table 4). Conversely, the pseudo-second-order model yielded a theoretical $q_e$ value of 23.15 mg/g, closely matching the experimental value of 23.0 mg/g. The high degree of correlation between these values suggests that the adsorption process follows a pseudo-second-order kinetic mechanism. Furthermore, the linear regression analysis for the pseudo-second-order plot demonstrated a high determination coefficient $R^2$, further confirming the model's applicability. This close agreement suggests that the adsorption of MB onto camel bone HAp is not a purely physical interaction (e.g., van der Waals forces) but rather governed by chemical adsorption mechanisms. Specifically, hydroxyapatite surfaces are known to have active calcium ($Ca^{2+}$) and phosphate ($PO_4^{3-}$) groups, which can interact with cationic dye molecules

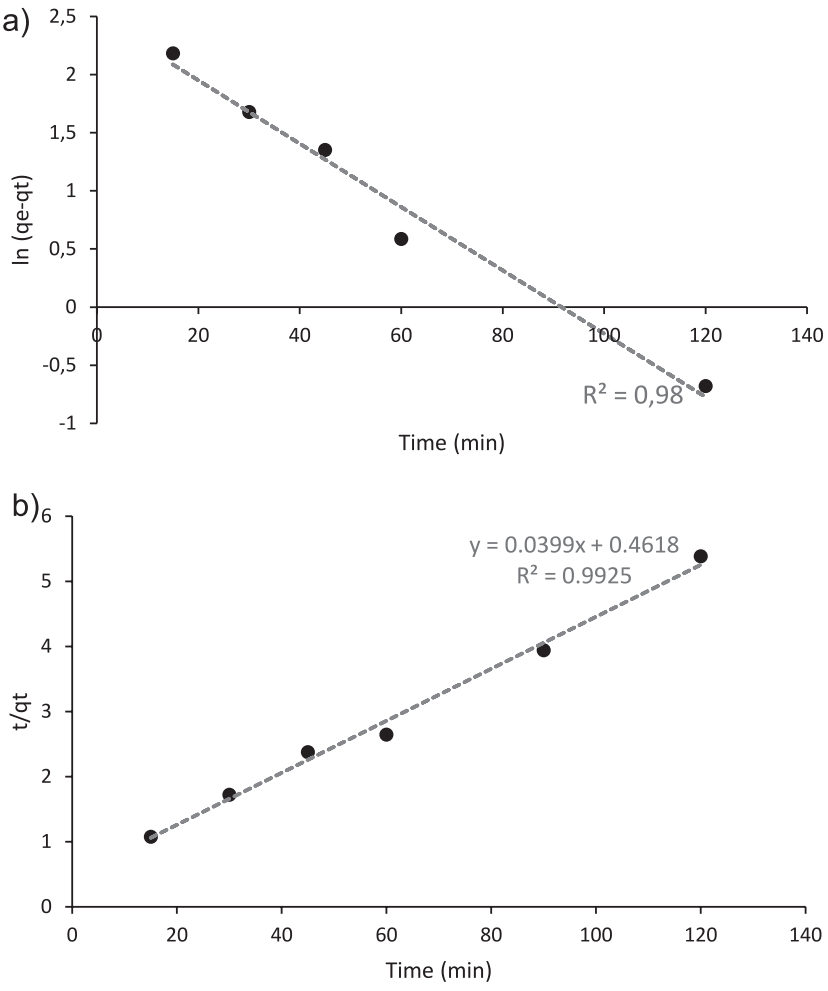


Fig. 8. a) Pseudo-first-order and b) Pseudo-second-order kinetic models.

Table 4. Kinetic parameters and correlation coefficients for MB adsorption on camel bone.

| Pseudo-first-order | | Pseudo-second-order | | Experimental $q_e$ |
|---|---|---|---|---|
| $q_e$, cal. (mg/g) | 16 | $q_e$, cal. (mg/g) | 23.15 mg/g | 23 (mg/g) |
| $K_1$ ($min^{-1}$) | -0.001 | $K_2$ ($min^{-1}$) | 2.04 | |
| $R^2$ | 0.98 | $R^2$ | 0.9925 | |

such as MB through ion exchange, where cationic dye molecules may partially replace $Ca^{2+}$ ions on the HAp surface; electrostatic attraction, as the negatively charged phosphate groups on the HAp surface attract the positively charged MB; and hydrogen bonding and surface complexation, where MB functional groups (e.g., amines or sulfur-containing moieties) form chemical interactions with surface hydroxyl (-OH) or phosphate groups. Thus, the pseudo-second-order model not only fits the data statistically but also reflects the underlying chemisorptive nature of the adsorption process between MB and camel bone-derived Hap [32].

## Thermodynamic Study

The following formula was used to determine thermodynamic factors, including the change in Gibb's free energy (ΔG°), enthalpy (ΔH°), and entropy (ΔS°). The following is the expression for the ΔG°: The following formula was used to determine thermodynamic factors such as the change in Gibb's free energy (ΔG°), enthalpy (ΔH°), and entropy (ΔS°). The following is the expression for the ΔG°:

$$\Delta G = -RTlnK \tag{8}$$

$$lnK_{ads} = \frac{\Delta S}{R} - \frac{\Delta H}{RT} \tag{9}$$

where ΔH° displays the variation in enthalpy having unit kJ/mol and ΔS° is the alteration in entropy having unit J/mol K (Table 5).

The thermodynamic parameters for the adsorption process were determined using the Van't Hoff Equation. The calculated enthalpy change (ΔH°) was 16614 kJ/mol, indicating that the adsorption process is endothermic, as energy is absorbed during the adsorption of methylene blue onto the adsorbent. A positive value suggests that adsorption is facilitated by an increase in temperature. The entropy change (ΔS°) was found to be 64 J/mol·K, indicating enhanced randomness at the solid-liquid interface throughout the adsorption process. This increase may be attributed to the displacement of water molecules from the adsorbent surface by methylene blue molecules, enhancing the disorder in the system [32, 33].

Table 5. Thermodynamic parameters for MB adsorption on camel dung.

| T (K) | ΔG° (J/mol) | ΔH° (J/mol) | ΔS° (J/mol.k) |
|---|---|---|---|
| 303 | -9826 | 16614 | 64 |
| 323 | -11362 | | |
| 343 | -12036 | | |
| 363 | -12066 | | |

The Gibbs free energy changes (ΔG°) at different temperatures were negative, ranging from -9826.0 J/mol at 303 K to -12066.0 J/mol at 363 K. The negative ΔG° values confirm that the adsorption process is spontaneous under the studied temperature range. Furthermore, the decreasing trend in ΔG° with increasing temperature indicates that the process becomes more thermodynamically favorable at higher temperatures, supporting the endothermic nature suggested by the positive ΔH° value. Overall, the thermodynamic analysis reveals that the adsorption of methylene blue onto the adsorbent is a spontaneous, endothermic process driven by enthalpy contribution, making the adsorption more efficient at elevated temperatures.

## Conclusions

In conclusion, this study successfully demonstrated the potential of camel bone-derived hydroxyapatite as an environmentally sustainable and efficient adsorbent for removing methylene blue dye from aqueous solutions. The adsorbent was prepared through a straightforward and eco-friendly process involving calcination and characterization, yielding a material with favorable structural and adsorption properties. The adsorption performance was evaluated through batch experiments, which explored the effects of critical parameters including adsorbent dosage, contact time, initial dye concentration, and temperature. The adsorption process followed the pseudo-second-order kinetic model with a high correlation coefficient ($R^2 = 0.99$). The equilibrium data were best fitted to the Langmuir isotherm model, confirming monolayer adsorption. Thermodynamic analysis revealed that the adsorption process was endothermic (ΔH° = 16.61 kJ/mol), indicating that the adsorption efficiency increased with temperature. The positive entropy change (ΔS° = 64.35 J/mol·K) suggested increased randomness at the solid-liquid interface, while the negative Gibbs free energy values (ΔG°) confirmed the spontaneous nature of

the adsorption process. Overall, the results demonstrate that camel bone-derived hydroxyapatite is a cost-effective and sustainable adsorbent with promising potential for wastewater treatment applications. Its effective adsorption capacity, coupled with environmental sustainability, positions it as a valuable alternative for removing dyes and other pollutants from contaminated water sources.

Future research should investigate the adsorbent's capacity to remove other classes of dyes, including anionic and azo dyes, as well as heavy metal ions and pharmaceutical contaminants. Moreover, the long-term stability and regeneration potential of the material over many reuse cycles need to be systematically evaluated to ensure durability. Another important direction is to assess the material's performance under real wastewater conditions, including complex matrices and competing ions. Pilot-scale or semi-industrial trials could provide practical insights into scalability and cost efficiency in real-world applications. These future directions will help expand the applicability of this low-cost, sustainable material and reinforce its potential as a viable solution for decentralized and eco-friendly wastewater treatment, particularly in arid and semi-arid regions where camel bone waste is readily available.

## Conflict of interest

The authors declare no conflict of interest.

## References


1. Al-TOHAMY R., ALI S.S., LI F., OKASHA K.M., MAHMOUD Y.A.G., ELSAMAHYl T., JIAO H., FU Y., SUN J. A critical review on the treatment of dye-containing wastewater: Ecotoxicological and health concerns of textile dyes and possible remediation approaches for environmental safety. Ecotoxicology and Environmental Safety. **231**,11360, **2022**.
2. JAWAD A.H., SAHU U.K., MASTULI M.S., ALOTHMAN Z.A., WILSON L.D. Multivariable optimization with desirability function for carbon porosity and methylene blue adsorption by watermelon rind activated carbon prepared by microwave assisted H3PO4. Biomass Conversion and Biorefinery. **14**, 577, **2024**.
3. BAKAR A.A.A., NOR AZMI N.F.A., MAT DAUD N., MUHAMMAD K.A., BADREALAM S., HAMZAH N. The removal of dye from synthetic wastewater using hybrid modified sugarcane bagasse-banana stem. IOP Conf. Environmental Earth Sciences. **1135**, 012010**, 2023**.
4. SANOSH K.P., CHU M.-C., BALAKRISHNAN A., KIM T.N., CHO S.-J. Utilization of biowaste eggshells to synthesize Nanocrystalline hydroxyapatite powders. Materials. **63**, 2100, **2009**.
5. SOLAYMAN H.M., HOSSEN M.A., ABDAZIZ A., YAHYA N.Y., LEONG K.H., SIM L.C., MONIR M.U., ZOH K.D. Performance evaluation of dye wastewater treatment technologies: A review. The Journal of Environmental Chemical Engineering. **11**, 109610, **2023**.
6. FOROUGHI M., PEIGHAMBARDOUST S.J., RAMAVANDI B., FOROUTAN R., PEIGHAMBARDOUSTN. S. Simultaneous degradation of methyl orange and indigo carmine dyes from an aqueous solution using nanostructured $WO_3$ and CuO supported on Zeolite 4°. Separation and Purification Technology. **344**, 127265, **2024**.
7. WU S.-C., HSU H.-C., HSU S.-K., CHANG Y.-C., HO W.-F. Synthesis of hydroxyapatite from eggshell powders through ball milling and heat treatment. Journal of Asian Ceramic Societies. **164**, 85, **2016**.
8. STOLZ A. Basic and applied aspects in the microbial degradation of azo dyes. Applied Microbiology and Biotechnology. **56**, 69**, 2001**.
9. LIAQAT M., MUNIR R.M., MARYAM I., IQBAL T., AFSHEENF S., NABI A.G., KHAN R.R.M., El-MARGHANY A., WARAD I., BASIT A. Synthesis and Characterization of $WO_3$/$BiVO_4$/Graphene Ternary Nanocomposites for the Photodegradation of Methlyene Blue and Tetracycline. Materials Chemistry and Physics. **320**, 129465, **2024**.
10. HAMAD H.N., IDRUS S. Recent developments in the application of bio-wastederived adsorbents for the removal of methylene blue from wastewater: a review. Polymers. **14**, 783, **2022**.
11. INGOLE V.H., HUSSEIN K.H., KASHALE A.A., GATTU K.P., DHANAYAT S.S., VINCHURKAR A., CHANG J., GHULE A.V. Invitro Bioactivity and Osteogenic Activity Study of Solid State Synthesized Nano-Hydroxyapatite Using Recycled Eggshell Bio–Waste. Chemistry Select. **1**, 3901, **2016**.
12. KOOHI P., RAHBAR-KELISHAMI A., SHAYESTEH H. Efficient removal of congo red dye using $Fe_3O_4$/NiO nanocomposite: Synthesis and characterization. Environmental Technology & Innovation. **23**, 101559, **2021**.
13. DEB A., DAS S., DEBNATH A. Fabrication and characterization of organometallic nanocomposite for efficient abatement of dye laden wastewater: CCD optimization, adsorption mechanism, co-existing ions, and cost analysis. Chemical Physics Letters. **830**, 140820, **2023**.
14. DAS S., PAUL S.R., DEBNATH A. Fabrication of biochar from jarul (Lagerstroemia speciosa) seed hull for ultrasound aided sequestration of ofloxacin from water: Phytotoxic assessments and cost analysis. Journal of Molecular Liquids. **387**, 122610, **2023**.
15. RASHED M.N., GAD A.A.E.M., FATHY N.M. Efficiency of chemically activated raw and calcined waste fish bone for adsorption of Cd (II) and Pb (II) from polluted water. Biomass Conversion and Biorefinery. **1**, 1, **2023**.
16. IBRAHIM M., LABAKI M., GIRAUDON J.M., LAMONIER J.F. Hydroxyapatite, a multifunctional material for air, water and soil pollution control: A review. The Journal of Hazardous Materials. **383**, 121139, **2020**.
17. TAREKEGN M.M., BALAKRISHNAN R.M., HIRUY A.M., DEKEBO A.H. Removal of methylene blue dye using nano zerovalent iron, nanoclay and iron impregnated nanoclay – a comparative study. RSC Advance. **11**, 30109, **2021**.
18. PUQI J., HONGWEI T., KUIREN L., WEI G. Removal of Methylene Blue from Aqueous Solution by Bone Char. Applied Sciences. **8**, 1903, **2018**.
19. BARUA E., DEOGHARE A.B., CHATTERJEE S., SAPKAL P. Effect of ZnO reinforcement on

the compressive properties, in vitro bioactivity, biodegradability and cytocompatibility of bone scaffold developed from bovine bone-derived HAp and PMMA. Ceramics International. **45**, 20331, **2019**.
20. GOPI D., BHUVANESHWARI N., INDIRA J., KANIMOZHI K., KAVITHA L. A novel green template assisted synthesis of hydroxyapatite Nanorods and their spectral characterization. Spectrochimica Acta, Part A: Molecular and Biomolecular Spectroscopy. **107**, 19, **2013**.
21. HAMEED B.H., AHMAD A.A., AZIZ N., Isotherms, kinetics and thermodynamics of acid dye adsorption on activated palm ash. Chemical Engineering Journal. **133**, 195, **2007**.
22. AADDOUZ M., AZZAOUI K., AKARTASSE N., MEJDOUBI E., HAMMOUTI B., TALEB M., SABBAHI R., ALSHAHATEETl S.F. Removal of methylene blue from aqueous solution by adsorption onto hydroxyapatite nanoparticles. Journal of Molecular Structure. 1288, **2023**.
23. DESALEGN Y.M., BEKELE E.A., OLU F.E. Optimization of Cd (II) removal from aqueous solution by natural hydroxyapatite/bentonite composite using response surface methodology. Scientific Reports. **13**, 5158, **2023**.
24. MALL I.D., SRIVASTAVA V.C., AGARWAL N.K. Removal of Orange-G and methyl violet dyes by adsorption onto bagasse Fly ash – kinetic study and equilibrium isotherm analyses. Dyes Pigments. **69**, 210, **2006**.
25. SENTHILKUMAAR S., VARADARAIAN P.R., PORKODI K., SUBBHURAAM C.V. Adsorption of methylene blue onto jute Fiber carbon: kinetics and equilibrium studies. Journal of Colloid and Interface Science. **284**, 78, **2005**.
26. HADDAD M.E., SLIMANI R., MAMOUNI R., ELANTRI S., LAZAR S. Removal of two textile dyes from aqueous solutions onto calcined bones. Journal of the Association of Arab Universities for Basic and Applied Sciences. **14**, 51, **2013**.
27. BENDAHO D., DRISS T.A., BASSOU D. Adsorption of acid dye onto activated Algerian clay. Bulletin of the Chemical Society of Ethiopia. **31**, 51, **2017**.
28. BARUA E., DEOGHARE A.B., CHATTERJEE S., SAPKAL P. Effect of ZnO reinforcement on the compressive properties, in vitro bioactivity, biodegradability and cytocompatibility of bone scaffold developed from bovine bone-derived HAp and PMMA. Ceramics International. **45**, 20331, **2019**.
29. RASHED M.N., GAD A.A., FATHY N.M. Efficiency of chemically activated raw and calcined waste fish bone for adsorption of Cd(II) and Pb(II) from polluted water. Biomass Conversion and Biorefinery. **13**, 1, **2023**.
30. DAS S., PAUL S.R., DEBNATH A. Fabrication of biochar from jarul (*Lagerstroemia speciosa*) seed hull for ultrasound aided sequestration of ofloxacin from water: Phytotoxic assessments and cost analysis. Journal of Molecular Liquids. **387**, 122610, **2023**.
31. IBRAHIM M., LABAKI M., GIRAUDON J.M., LAMONIER J.F. Hydroxyapatite, a multifunctional material for air, water and soil pollution control: A review. Journal of Hazardous Materials. **383**, 1211139, **2020**.
32. HAN X., WANG W., MA X. Adsorption characteristics of methylene blue onto low cost biomass material Lotus leaf. Chemical Engineering Journal. **171**, 1, **2011**.
33. SIRAJUDHEEN P., KARTHIKEYAN P., VIGNESHWARAN S., MEENAKSHI S. Complex interior and surface modified alginate reinforced reduced graphene oxide-hydroxyapatite hybrids: removal of toxic azo dyes from the aqueous solution. International Journal of Biological Macromolecules. **175**, 361, **2021**.